Structural Engineering and Mechanics, *Vol. 55, No. 3 (2015) 555-581*
DOI: http://dx.doi.org/10.12989/sem.2015.55.3.555

Shape optimization for partial double-layer spherical reticulated shells of pyramidal system

J. Wu[1,2a], X.Y. Lu[2b], S.C. Li[1c], D.L. Zhang[3d], Z.H. Xu[*1], L.P. Li[1e] and Y.G. Xue[1f]

[1]Geotechnical and Structural Engineering Research Center, Shandong University, Ji'nan 250061, Shandong, China
[2]Institute of Engineering Mechanics, Shandong Jianzhu University, Ji'nan 250101, Shandong, China
[3]Shandong Agriculture and Engineering University Ji'nan 250100, Shandong, China

(Received February 1, 2015, Revised April 5, 2015, Accepted May 15, 2015)

Abstract. Triangular pyramid and Quadrangular pyramid elements for partial double-layer spherical reticulated shells of pyramidal system are investigated in the present study. Macro programs for six typical partial double-layer spherical reticulated shells of pyramidal system are compiled by using the ANSYS Parametric Design Language (APDL). Internal force analysis of six spherical reticulated shells is carried out. Distribution regularity of the stress and displacement are studied. A shape optimization program is proposed by adopting the sequence two-stage algorithm (RDQA) in FORTRAN environment based on the characteristics of partial double-layer spherical reticulated shells of pyramidal system and the ideas of discrete variable optimization design. Shape optimization is achieved by considering the objective function of the minimum total steel consumption, global and locality constraints. The shape optimization of six spherical reticulated shells is calculated with the span of 30m~120m and rise to span ratio of 1/7~1/3. The variations of the total steel consumption along with the span and rise to span ratio are discussed with contrast to the results of shape optimization. The optimal combination of main design parameters for six spherical reticulated shells is investigated, i.e., the number of the optimal grids. The results show that: (1) The Kiewitt and Geodesic partial double-layer spherical reticulated shells of triangular pyramidal system should be preferentially adopted in large and medium-span structures. The range of rise to span ratio is from 1/6 to 1/5. (2) The Ribbed and Schwedler partial double-layer spherical reticulated shells of quadrangular pyramidal system should be preferentially adopted in small-span structures. The rise to span ratio should be 1/4. (3) Grids of the six spherical reticulated shells can be optimized after shape optimization and the total steel consumption is optimized to be the least.

Keywords: pyramidal system; APDL; parametric modeling; RDQA; shape optimization

---

∗Corresponding author, Lecturer, E-mail: zhenhao_xu@sdu.edu.cn
[a]Ph.D. Student, E-mail: wujing9516@163.com
[b]Professor, E-mail: lxy5504@sdjzu.edu.cn
[c]Professor, E-mail: lishucai@sdu.edu.cn
[d]M. Eng., E-mail: daliang08@sina.com
[e]Associate Professor, E-mail: yuliyangfan@163.com
[f]Professor, E-mail: xieagle@sdu.edu.cn

http://www.techno-press.org/?journal=sem&subpage=8 ISSN: 1225-4568 (Print), 1598-6217 (Online)

1. Introduction

Before the 19th century, spatial structure developed very slowly due to the restrictions of building materials and relevant technical. Later, it has got a fast development with the improvement of steel production technology, the rapid development of computer technology and the increasing social demand. Spherical reticulated shell as a new mesh style has also been widely used (Svanberg 1987, Saka 1991, Salajegheh and Vanderplaats 1993).

Spherical reticulated shells are spatial skeletal structures, and their rod-system is generated by connecting the nodes according to certain rules. Owing to their good appearance, reasonable stress and large stiffness (Shen and Chen 1996, Deng and Dong 1999), they have vast application prospects in modern large-span building structures (Rajan1995, Dong and Yao 2003), such as major sports / arts venues, waiting halls and shopping malls (Fig. 1).

According to different grid types, there are six typical spherical reticulated shells, i.e., Ribbed spherical reticulated shell, Schwedler spherical reticulated shell, Lamella spherical reticulated shell, Three-way grid spherical reticulated shell, Kiewitt spherical reticulated shell and Geodesic spherical reticulated shell. Spherical reticulated shells can also be divided into single-layer, double-layer, partial double-layer etc. based on their structural type. Partial double-layer spherical reticulated shell of pyramidal system is a reinforced structural style on the basis of single-layer spherical reticulated shell, which is generated by connecting the nodes according to certain rules base on triangular pyramid and quadrangular pyramid. Partial double-layer spherical reticulated shells of pyramidal system combine the virtues of single-layer and double-layer spherical reticulated shells (Levy *et al*. 1994, He *et al*. 2002). They have higher integral bearing capacity and deformation resistant capability than single-layer spherical reticulated shells, and their total weight is less than double-layer spherical reticulated shells. Therefore, partial double-layer spherical reticulated shells of pyramidal system are typical and widely used structures in modern architectures. However, the number of nodes and rod elements of spherical reticulated shells is too many and the variation of span, rise, grid size, type and other parameters can cause structural internal force reallocation. Besides, the workload of re-modeling is very large and it is quite difficult to carry out high efficient internal force analysis and shape optimization design. Conventional modeling of these structures often relies on hand-modeling rather than on parametric modeling in domestic and foreign studies. Relevant research is also seldom related to the specific

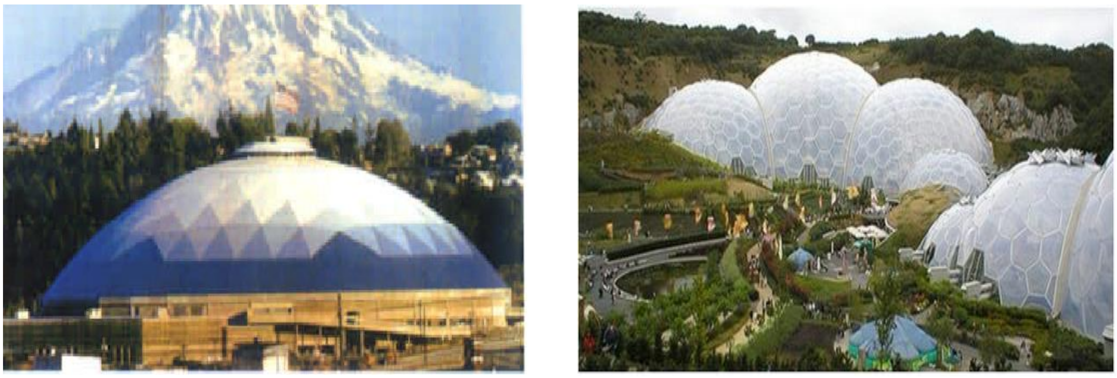

(a) Gymnasium of America Tacoma (b) Eden project of England

Fig. 1 Examples of spherical reticulated shells work of shape optimization design. In addition, these structural materials are ideal but of high cost. Thus, shape optimization is quite necessary and important for the design and construction of spherical reticulated shells (Yas *et al*. 2007, Lu *et al*. 2012).

At present, continuous variable optimization design has already possessed perfect theoretical system and abundant practical experience, but the research on optimization design of discrete variable is not many. The present research achievements are mainly as follows: Jenkins studied structural optimization with the genetic algorithm (1991) and natural algorithm (1997). Saka and Kameshki (1998) investigated optimum design of nonlinear elastic framed domes, i.e., an algorithm was presented for the optimum design of three-dimensional rigidly jointed frames which took into account the nonlinear response due to the effect of axial forces in members. He *et al*. (2001) proposed that chaos optimization algorithm could be used in the optimization design of double-layer cylindrical reticulated shell, which realized the synchronous optimization of the rise to span ratio, grid size and vault thickness as continuous variables. Zhang and Dong (2003) presented a structural optimization algorithm. In the process of optimum design, both the stress constraints and displacement constraints were considered. The geometrical nonlinearity was taken into account during the computation of stresses and displacements. A computer program was developed, and the design example verified the effectiveness of the proposed method. Xu *et al*. (2006) investigated an optimal method, and this optimum design was performed by the combination of the direct searching method and the criterion. Wang and Tang (2006) proposed an optimum method based on the optimality criteria, which could be used in optimization design of single-layer reticulated shells. The constraints of displacement, stress, member stability and structural stability were considered. Vyzantiadou *et al*. (2007) proposed structural systems. The proposed computational method produced algorithms using fractal mathematics, and could generate forms applicable to shells. Yas *et al*. (2007) proposed the stacking sequence optimization of a laminated cylindrical shell for obtaining maximum natural frequency and buckling stress, simultaneously. Rahami *et al*. (2008) introduced a combination of energy and force method, and genetic algorithm was employed as an optimization tool for minimizing the weight of the truss structures. Wu *et al*. (2010) investigated a new design concept of MAS, and a shape optimization method with finite element analysis was applied on two-dimensional (2D) stent models. Durgun and Yildiz (2012) introduced a new optimization algorithm, called the Cuckoo Search Algorithm, for solving structural design optimization problems. Luo *et al.* (2012) also studied a meshless Galerkin level set method for shape and topology optimization of continuum structures. Yildiz (2013) investigated a comparison of evolutionary-based optimization techniques for structural design optimization problems. Furthermore, a hybrid optimization technique based on differential evolution algorithm was introduced for structural design optimization problems. Emmanuel *et al.* (2014) used ANN and GA for buckling optimization of laminated composite plate with elliptical cutout. In addition, the publications (Kaveh and Zolghadr 2014, Kaveh and Ahmadi2014, Thall *et al*. 2014) also considered the structural optimization design.

In the present study, generation methods of nodes and rod elements for six typical partial double-layer spherical reticulated shells of pyramidal system are proposed. Macro programs are compiled by using the ANSYS Parametric Design Language (APDL). Users can easily get the required models only by inputting five parameters, i.e., the shell span (*S*), rise (*F*), latitudinal portions (*Kn*), radial loops (*Nx*) and thickness of double-layer (*T*). The purpose of rapid modeling can be attained by modifying parameters simply. The method can greatly improve efficiency of internal force analysis and optimization design, and reduce analyzing cost. It lays good foundation for structural internal force analysis and shape optimization. Then the maximum stress and displacement of six typical spherical reticulated shells are analyzed. Moreover, a shape optimization program is proposed based on the sequence two-stage algorithm in FORTRAN environment. The shape optimization of six typical spherical reticulated shells are calculated with the span of 30 m~120 m and rise to span ratio of 1/7~1/3. The variations of the total steel consumption along with the span and rise to span ratio are discussed with contrast to the results of shape optimization. The optimal combined regulation of main design parameters is studied. The research results provide reference for actual spherical reticulated shells.

2. The types of partial double-layer spherical reticulated shells of pyramidal system

According to different grid styles, spherical reticulated shells can be divided into six types, i.e., Ribbed type, Schwedler type, Lamella type, Three-way grid type, Kiewitt type and Geodesic type. For the first three spherical reticulated shells, the basic unit of partial double-layer is quadrangular pyramid. For the latter three spherical reticulated shells, the basic unit of partial double-layer is triangular pyramid. The position of vertex for a pyramid is determined by the bottom surface and the height of a pyramid, i.e., the upper layer grids of spherical reticulated shells and the thickness of partial double-layer. Triangular pyramid system and quadrangular pyramid system are formed by connecting vertex and each point on the bottom surface (Zhang 2014). The basic unit of pyramidal system and actual pyramidal system are shown in Figs. 2-3.

(a) The basic unit of triangular pyramid (b) The basic unit of quadrangular pyramid

Fig. 2 The basic unit of pyramidal system

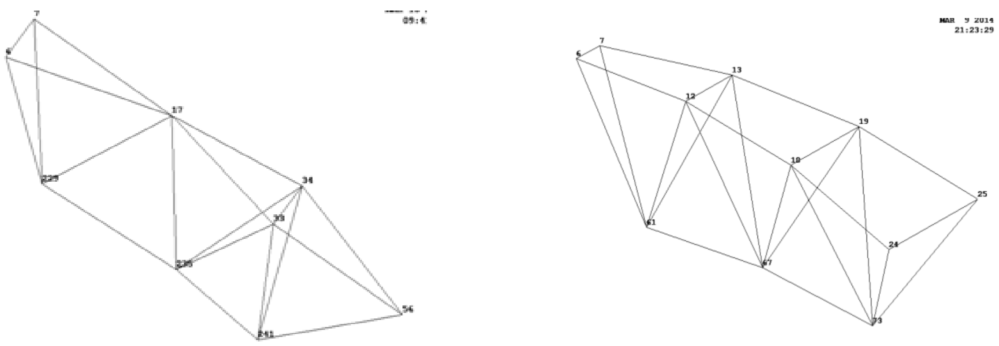

(a) Triangular pyramid system (b) Quadrangular pyramid system

Fig. 3 Pyramidal system

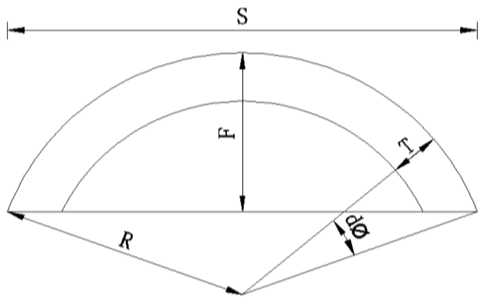

Fig. 4 Geometric parameters schematic diagram of spherical reticulated shells

Six typical partial double-layer spherical reticulated shells of pyramidal system are studied, i.e., Ribbed partial double-layer spherical reticulated shells of quadrangular pyramid system, Schwedler partial double-layer spherical reticulated shells of quadrangular pyramid system, Lamella partial double-layer spherical reticulated shells of quadrangular pyramid system, Three-way grid partial double-layer spherical reticulated shells of triangular pyramid system, Kiewitt partial double-layer spherical reticulated shells of triangular pyramid system, Geodesic partial double-layer spherical reticulated shells of triangular pyramid system.

3. Parametric modeling

3.1 Geometric descriptions

The main geometric parameters (Fig. 4) of describing spherical reticulated shells have: shell span(*S*), rise (*F*), latitudinal portions (*Kn*), radial loops (*Nx*), thickness of double-layer (*T*). The sphere curvature radius *R* is calculated (Shen and Chen 1996, Lu *et al.* 2013) by Eq. (1). The global angle *Dpha* of two radial neighboring circle nodes is calculated (Shen and Chen 1996, Lu *et al.* 2013) by Eq. (2).

$$R = \frac{\frac{S^2}{4} + F^2}{2F} \tag{1}$$

$$Dpha = \begin{cases} \arctan \dfrac{S}{2Nx\sqrt{R^2 - \left(\dfrac{S}{2}\right)^2}} & \dfrac{F}{S} \neq \dfrac{1}{2} \\ \dfrac{90}{Nx} & \dfrac{F}{S} = \dfrac{1}{2} \end{cases} \tag{2}$$

3.2 The methods of APDL parametric modeling

S, *F*, *Kn*, *Nx* and *T* are given in the spherical coordinates, then the sphere curvature radius *R* and global angle *Dpha* are calculated. The nodes are generated in each circle from inside to outside in order by using cyclic command statements. Spherical surface, quadrangular pyramid and triangular pyramid are formed by connecting the nodes. Displacement constraints and external loads are applied on the structures.

Taking Kiewitt partial double-layer spherical reticulated shells of triangular pyramid system as an example. Its modeling process is as follows: Let vertex of upper layer be number 1. Applying loads on nodes whose number is less than starting node number of the outermost circle and imposing displacement constraints on other nodes. Rod types, material properties, real constants, etc., are applied to analyze the structural internal force. Macro programs are compiled by using APDL in ANSYS (Chen and Liu 2009, Gong and Xie 2010, Zhang *et al.* 2013, Zhang 2014).The program's commands of generating nodes are *N*, *NODE*, *X*, *Y*, *Z* in ANSYS. Wherein the *X*, *Y*, *Z* are the coordinates of nodes. The program's commands of generating rod elements are *E*, P_1, P_2 in ANSYS. Wherein the P_1, P_2 are the node numbers on both ends of rod element.

(1) Determine the numbers and coordinates of nodes:

The number of upper layer nodes is Num_1=1+Kn×Nx×(Nx+1)/2. The j-th node at the i-th loop from the vertex to outside is numbered as 1+Kn×(i−1)×i/2+j, which coordinates are (R, (j−1)× 360/(Kn×i), 90−i×DPha). The number of lower layer vertex is Num_1+1. The j-th node at the i-th loop from inside to outside is numbered as 1+Kn×(i−1)+j+Num_1, which coordinates are (R-T, (j−0.5)×360/Kn, 90− (i−0.5)×DPha).

(2) Rod elements connection:

1) Rod elements connection of upper layer: The latitudinal rod elements at the i-th loop and the j-th portion (1≤j≤Kn×i−1) are made by connecting the node 1+Kn×(i−1)×i/2+j and the node 1+Kn×(i−1)×i/2+j+1. The latitudinal rod elements at the last portion (j=kn) of each loop are made by connecting the last node 1+Kn×(i−1)×i/2+1 and the first node 1+Kn×(i−1)×i/2+Kn×i of this loop. The radical rod elements of the first loop are made by connecting the vertex and nodes of the first loop. Then, all the rest of radial rod elements are made by adopting two-level circulating modes, i.e., the portions circulating and internal rod elements circulating.

2) Rod elements connection of lower layer:

Firstly, the triangular pyramid vertexes between upper layer and lower layer are connected.

Secondly, the triangular pyramids between the first loop and second loop are connected solely. Starting from the third loop, the triangular pyramids of odd-numbered loops are made by connecting vertexes of lower layer Num_1+1+(i−1)×Kn+j and three nodes of upper layer (i-2)×(i−1)×Kn/2+(i−3)/2+3+(j−1)×(i-1), (i-1)×i×Kn/2+(i-3)/2+3+(j-1)×i and (i−1)×i×Kn/2+(i−3)/2+3+ (j−1)×i+1 respectively. The triangular pyramids of even-numbered loops are made by connecting vertexes of lower layer Num_1+1+(i−1)×Kn+j and three nodes of upper layer i×(i−1)×Kn/2+i/2+2+(j−1)×i, (i−1)×(i−2)×Kn/2+i/2+1+(j−1)×(i−1) and (i−1) ×(i−2)×Kn/2+i/2+2+ (j−1)×(i−1) respectively.

Thirdly, in the j-th portion (1≤j≤Kn−1) between the second loop and third loop, the rod elements are made by connecting the node Num1+1+(i−1)×Kn+j and two nodes i×(i−1)×Kn/2+ i/2+1+(j−1)×i, i×(i−1)×Kn/2+i/2+1+(j−1)×i+2 respectively. When j=Kn, the rod elements are made by connecting the node Num_1+1+(i−1)×Kn+j and the node 1+(i−1)×Kn+i/2. Starting from the fourth loop, the rod elements of even-numbered loops are made by connecting the node Num_1+ 1+(i−1)×Kn+j and two nodes i×(i−1)×Kn/2+i/2+1+(j−1)×i, i×(i−1)×Kn/2+i/2+1+(j−1)×i+2 respectively. Starting from the fifth loop, the rod elements of odd-numbered loops are made by connecting the node Num_1+1+(i−1)×Kn+j and two nodes (i−1)×(i−2)×Kn/2+(i−1)/2+1+(j−1)×(i−1), (i−1)×(i−2)×Kn/2+(i−1)/2+1+(j−1)×(i−1)+2 respectively. Finally, the radical rod elements of lower layer are made by connecting the node 1+Kn×(i−1)+j+Num_1 and the node 1+Kn×i+j+Num_1.

(3)Boundary constraints and nodal loads:

The starting node number of the outermost loop is $Num_1-Kn\times Nx+1$. Applying loads on nodes whose number is less than the number and imposing displacement constraints on other nodes.

3.3 The input window of geometrical parameters

Users can easily get the required models only by inputting parameters such as *S*, *F*, *Kn*, *Nx* and *T*. Procedures are as follows:

Customizing programs of geometrical parameters window

```
 MULTIPRO,'start',4
 *cset,1,3, S, ' Span=(mm)',90
 *cset,4,6, F, ' Rise =(mm)',18
 *cset,7,9, Kn, ' Latitudinal portions = ',16
 *cset,10,12, Nx, ' Radial loops =',8
 *cset,13,15, T, 'Thickness=(mm)',1
 *cset,61,62, 'Please input geometry parameters'
   MULTIPRO, 'end'
```

3.4 Modeling examples

Parametric modeling examples of six typical spherical reticulated shells are shown in Figs. 5-10.

4. The internal force analysis

As for spherical reticulated shells, the basal principle and methods of internal force analysis can be summarized as two categories. The first category is imitative shell method based on continuity assumption, and the second category is finite element method of truss structures based on discretization assumption. For imitative shell method, the structures are analyzed and studied

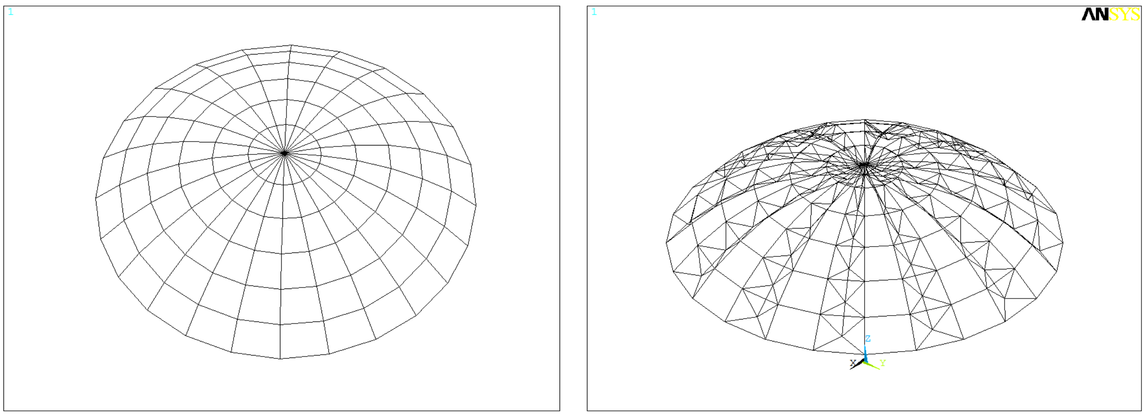

(a) Single-layer (b) Quadrangular pyramid system

Fig. 5 Ribbed spherical reticulated shell (*S*=30 m, *F*=7.5 m, *Kn*=24, *Nx*=6, *T*=0/1)

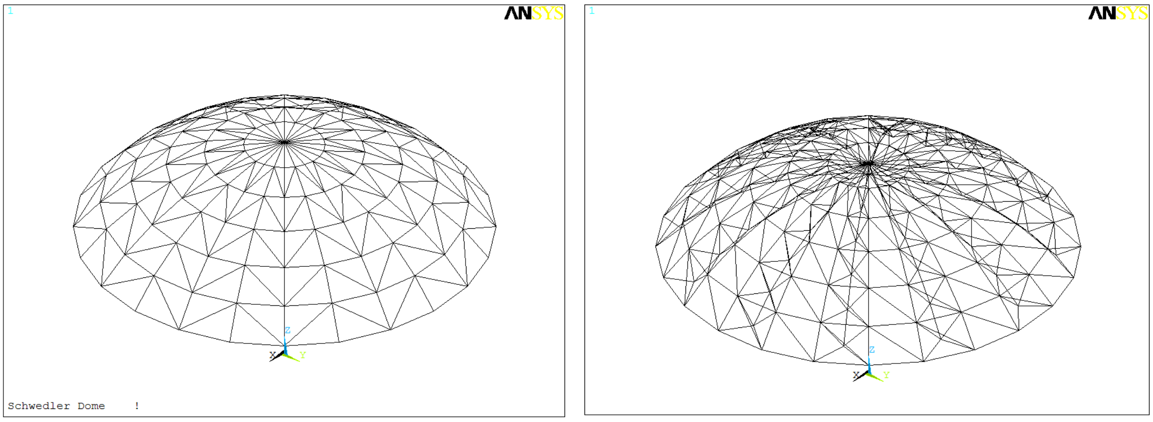

(a) Single-layer (b) Quadrangular pyramid system

Fig. 6 Schwedler spherical reticulated shell (S=30 m, F=7.5 m, Kn=24, Nx=6, T=0/1)

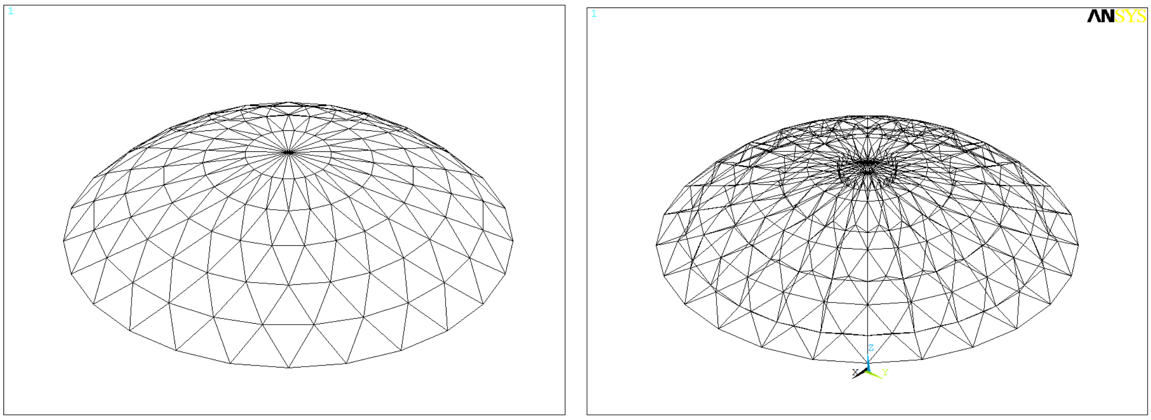

(a) Single-layer (b) Quadrangular pyramid system

Fig. 7 Lamella spherical reticulated shell (S=30 m, F=7.5 m, Kn=24, Nx=6, T=0/1)

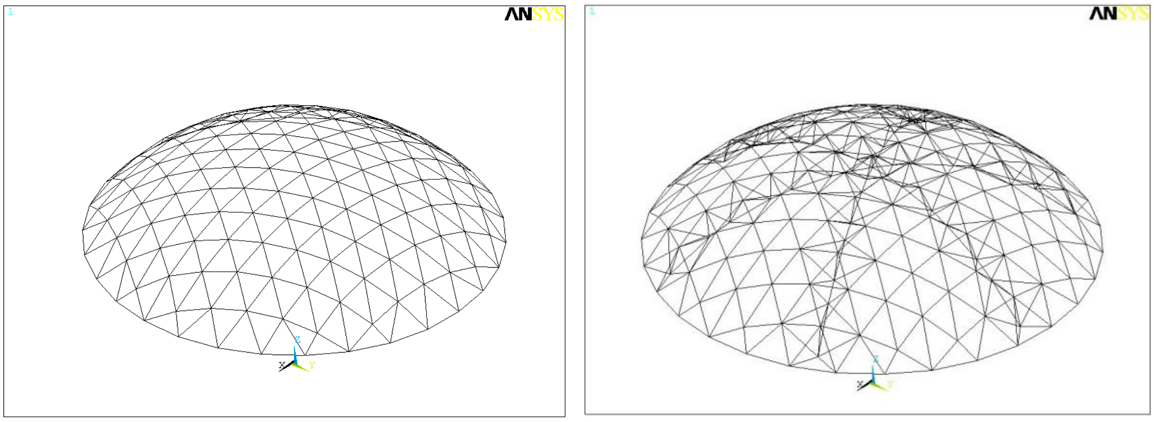

(a) Single-layer (b) Triangular pyramid system

Fig. 8 Three-way grid spherical reticulated shell (S=30 m, F=7.5 m, Kn=6, Nx=6, T=0/1)

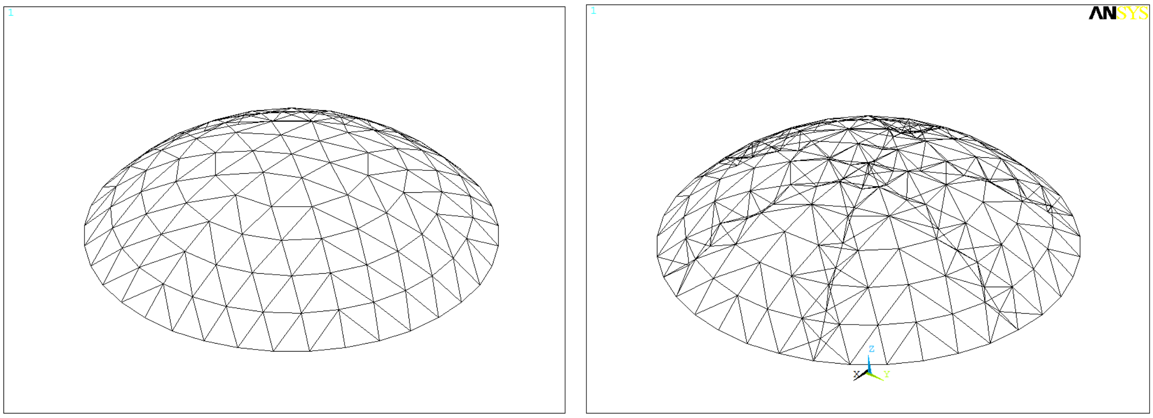

(a) Single-layer (b) Triangular pyramid system

Fig. 9 Kiewitt spherical reticulated shell (*S*=30 m, *F*=7.5 m, *Kn*=6, *Nx*=6, *T*=0/1)

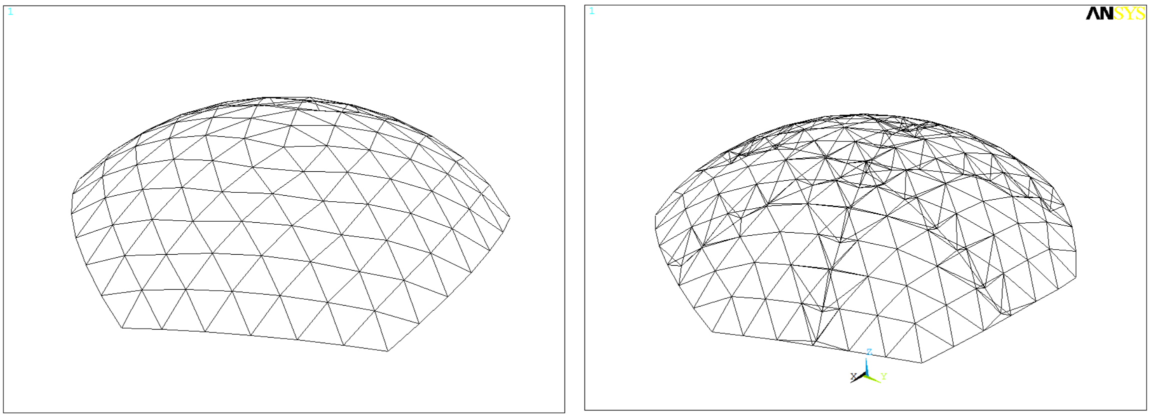

(a) Single-layer (b) Triangular pyramid system

Fig. 10 Geodesic spherical reticulated shell (*S*=30 m, *F*=7.5 m, *Kn*=6, *Nx*=6, *T*=0/1)

according to the basic theory of elastic thin shells. Its purpose is to obtain displacement and stress of the structures and then convert into internal force of spherical reticulated shells. The basal principle of finite element method for truss structures is that the grids constituted by rod elements originally can disperse into individual element. And a rod can be usually considered as a basic element when conducting internal force analysis.

The finite element method of truss structures is usually adopted when making internal force analysis for reticulated shells. This method can be applied in static, dynamic and buckling analysis of all types of spherical reticulated shells.

This study makes use of finite element analysis software (ANSYS) for internal force analysis of six typical spherical reticulated shells. Space beam elements are adopted as rod elements, and the nodes of spherical reticulated shells are assumed to be ideal rigid joints. Beam4 element is selected in the present study. Beam4 is a tensile and compressive, torsional and bending element in the axial direction, meanwhile, each node has six degrees of freedom, which can translate along the *X*, *Y*, *Z* directions and rotate around the *X*, *Y*, *Z* axis in the node coordinate system.

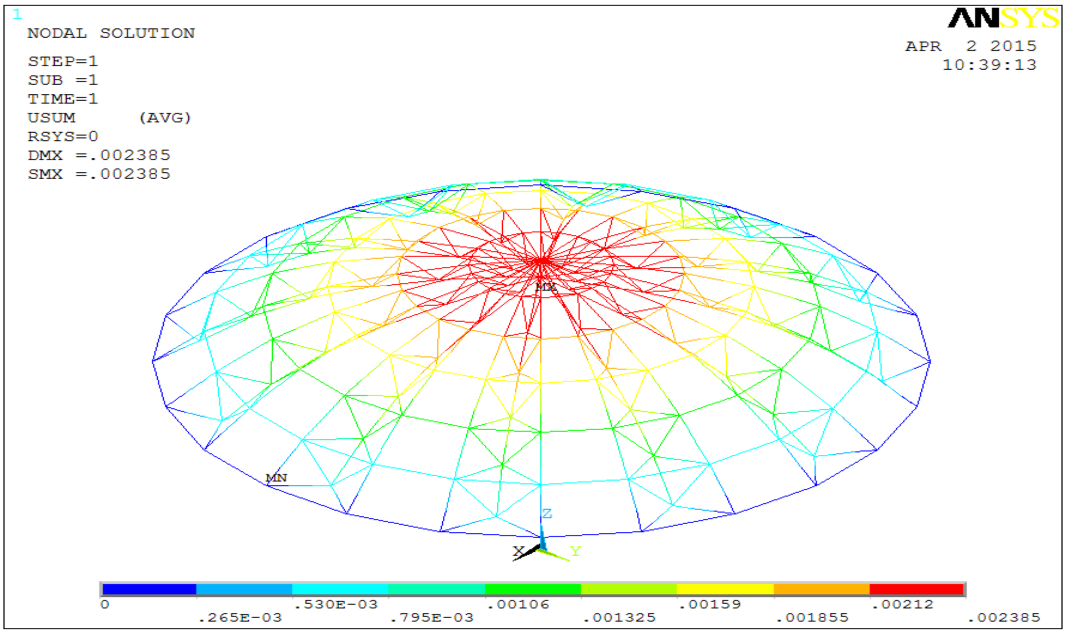

Fig. 11 Displacement contour of Ribbed partial double-layer spherical reticulated shells of quadrangular pyramid system (S=30 m, F=7.5 m, Kn=24, Nx=6, T=1)

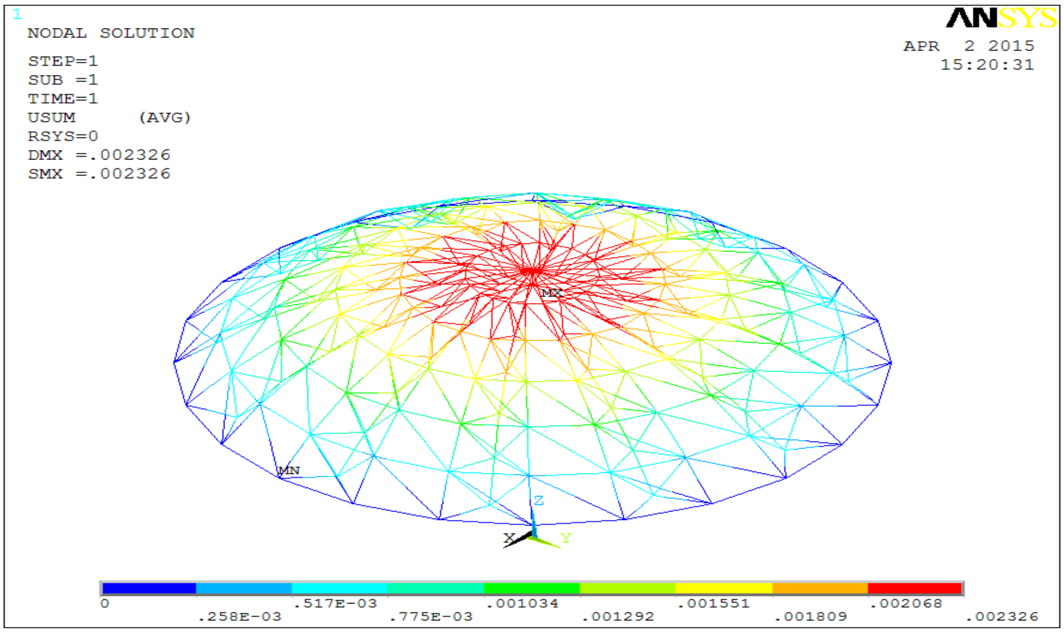

Fig. 12 Displacement contour of Schwedler partial double-layer spherical reticulated shells of quadrangular pyramid system (S=30 m, F=7.5 m, Kn=24, Nx=6, T=1)

The relevant parameters are unified, so that the calculated results are comparable. Rod elements of spherical reticulated shells adopt hot-rolling seamless pipe (calculated by YB 231-70), steel

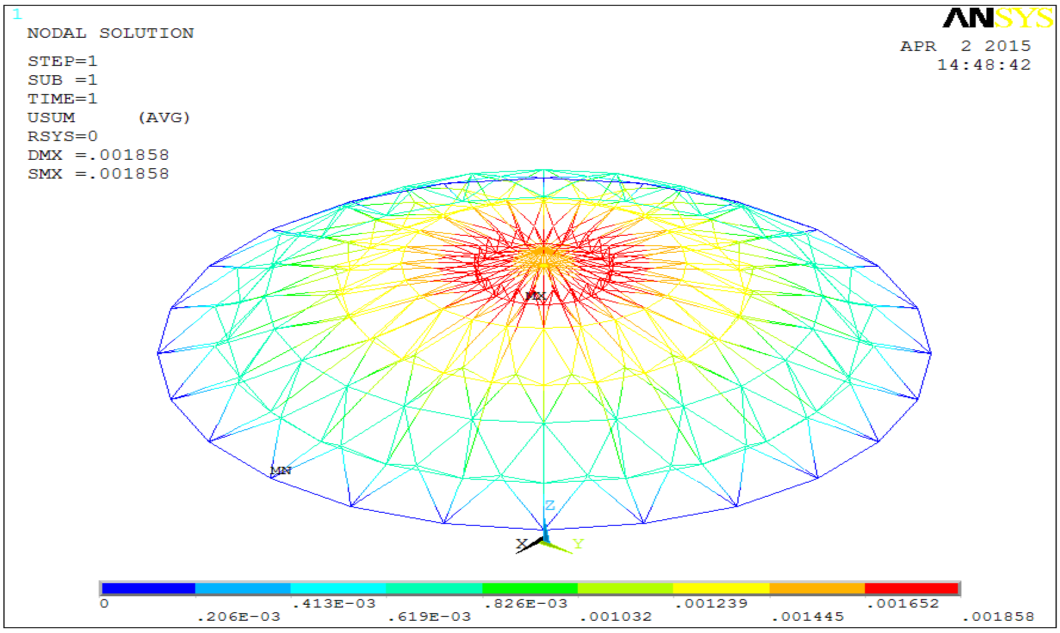

Fig. 13 Displacement contour of Lamella partial double-layer spherical reticulated shells of quadrangular pyramid system (S=30 m, F=7.5 m, Kn=24, Nx=6, T=1)

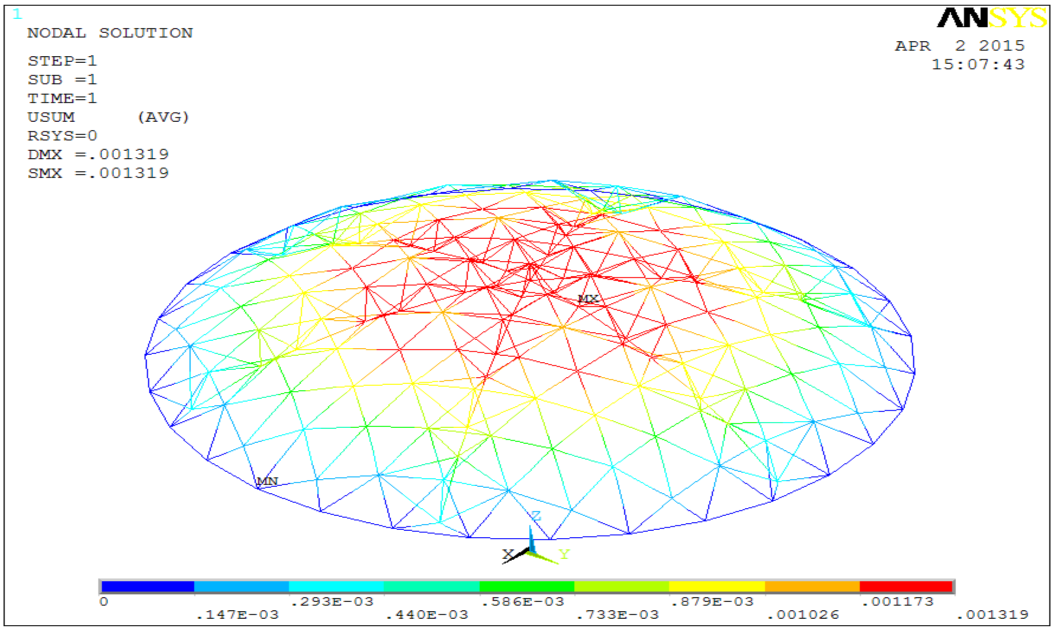

Fig. 14 Displacement contour of Three-way grid partial double-layer spherical reticulated shells of triangular pyramid system (S=30 m, F=7.5 m, Kn=6, Nx=6, T=1)

density ρ=7800 kg/m^3, elastic modulus E=2.06×10^5 Mpa, Poisson ratio ε=0.3, yield strength of steel $[\sigma]$=2.15×10^8 N/m^2. The steel type is Q235, i.e., outer diameter D=0.152 m, wall thickness

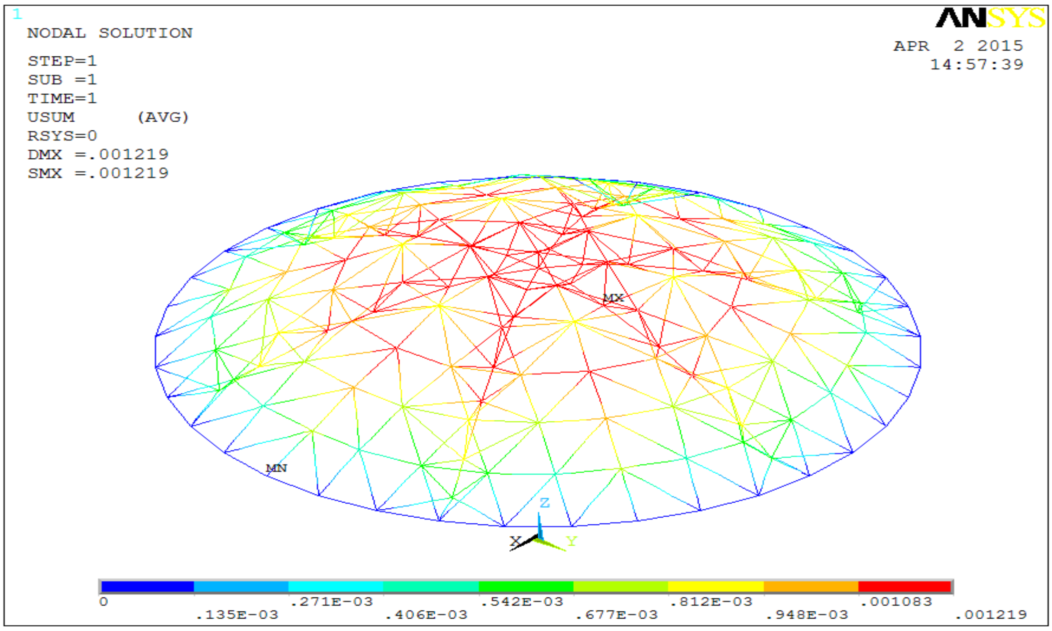

Fig. 15 Displacement contour of Kiewitt partial double-layer spherical reticulated shells of triangular pyramid system (S=30 m, F=7.5 m, Kn=6, Nx=6, T=1)

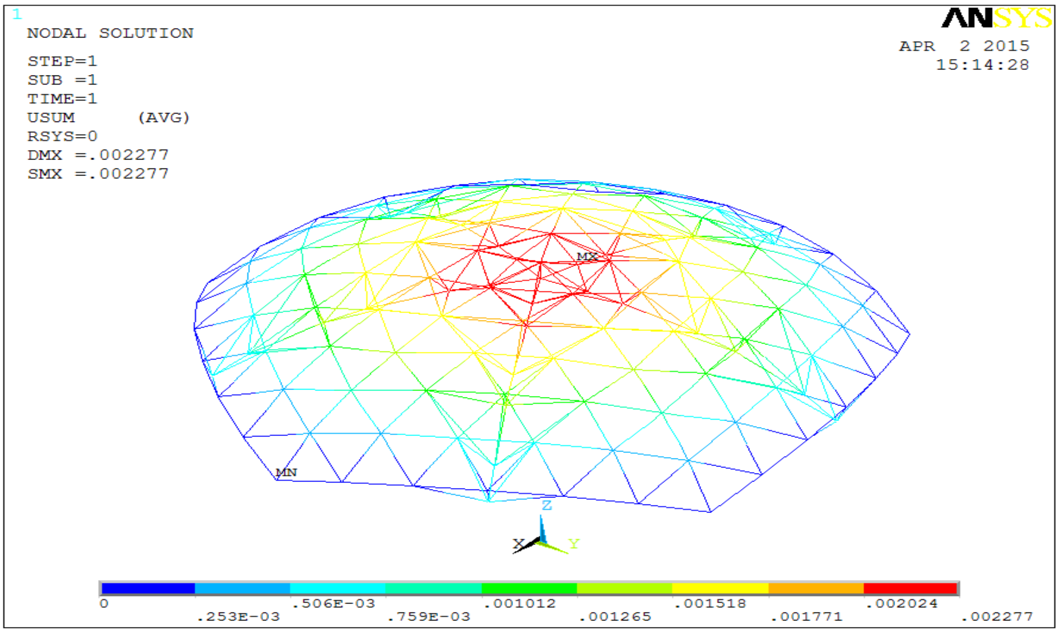

Fig. 16 Displacement contour of Geodesic partial double-layer spherical reticulated shells of triangular pyramid system (S=30 m, F=7.5 m, Kn=6, Nx=6, T=1)

t=4.5 mm, sectional area $S=2.085\times10^{-3}$ m^2, second moment of area $I=5.6761\times10^{-6}$ m^4, sectional resistance moment $W=7.469\times10^{-5}$ m^3.The equivalent uniformly distributed loads of roof (q=2.35

Table 1 The results of internal force analysis for six typical partial double-layer spherical reticulated shells of pyramidal system

Type	*S* (m)	*F* (m)	*Kn*	*Nx*	*T* (m)	The maximum displacement (m)	Allowed values (m)	The maximum stress (Mpa)	Allowed values (Mpa)
Ribbed type	30	7.5	24	6	1	0.002385	0.075	30.2	215
	60	15	36	12	1.5	0.016967	0.150	87.5	
	90	22.5	48	18	2	0.047365	0.225	152	
Schweder type	30	7.5	24	6	1	0.002326	0.075	31.2	215
	60	15	36	12	1.5	0.016574	0.15	91.3	
	90	22.5	48	18	2	0.046241	0.225	159	
Lamella type	30	7.5	24	6	1	0.001858	0.075	18.1	215
	60	15	36	12	1.5	0.012761	0.15	55.7	
	90	22.5	48	18	2	0.036384	0.225	107	
Three-way grid type	30	7.5	6	6	1	0.001319	0.075	18.5	215
	60	15	6	12	1.5	0.007478	0.15	43.9	
	90	22.5	6	18	2	0.019901	0.225	85.8	
Kiewitt type	30	7.5	6	6	1	0.001219	0.075	17.3	215
	60	15	6	12	1.5	0.006115	0.15	39.0	
	90	22.5	6	18	2	0.015245	0.225	58.0	
Geodesic type	30	7.5	6	6	1	0.002277	0.075	23.2	215
	60	15	6	12	1.5	0.009562	0.15	52.2	
	90	22.5	6	18	2	0.027537	0.225	76.2	

KN/m^2) vertically downward effect on the nodes of spherical reticulated shells. The allowable structural maximum displacement is 1/400 of the span (Technology Procedures of Space Grid Structure, 2010). In addition, constraint condition of the outermost nodes of spherical reticulated shells is simply supported, which cannot translate along the *X*, *Y*, *Z* directions but rotate around the *X*, *Y*, *Z* axis. The internal force analysis of six typical partial double-layer spherical reticulated shells of pyramidal system, in the span of 30 m, 60 m and 90 m, are calculated. Take displacement as an example, the displacement contours are shown in Figs. 11-16. Analysis results are shown in Table 1.

The following conclusions can be obtained from Figs. 11-16 and Table 1:

(1) Overall, as for the six typical partial double-layer spherical reticulated shells of pyramidal system, their maximum displacement and maximum stress both increase with the span. Take Ribbed partial double-layer spherical reticulated shells of quadrangular pyramid system as an example, when the span is 30 m, 60 m and 90 m, its maximum displacement are 0.002389 m，0.016967 m and 0.047365 m, in that order. In addition, its maximum stress are 30.2 MPa，87.5 MPa and 152 MPa, in that order.

(2) From the displacement of six typical spherical reticulated shells under the loads aspect, the maximum displacement of Ribbed spherical reticulated shell based on quadrangular pyramid is the biggest, followed by Schwedler spherical reticulated shell. The maximum displacement of Kiewitt spherical reticulated shell based on triangular pyramid is the smallest, followed by Geodesic spherical reticulated shell. The maximum displacement of Ribbed and Schwedler spherical reticulated shells occur at the vertex, and the rest of the four occur in the vicinity of the vertex.

(3) From the stress of six typical spherical reticulated shells under the loads aspect, the maximum stress of Schwedler spherical reticulated shell based on quadrangular pyramid is the biggest, followed by Ribbed spherical reticulated shell. The maximum stress of Kiewitt spherical reticulated shell based on triangular pyramid is the smallest, followed by Geodesic spherical reticulated shell. The stress variety of Ribbed, Schwedler and Lamella spherical reticulated shells is more obvious than the other three spherical reticulated shells. The stress distribution of Ribbed, Schwedler and Lamella spherical reticulated shells is also uneven, and the stress distribution of the other three spherical reticulated shells is relatively uniform.

(4) In the quadrangular pyramid system, Schwedler spherical reticulated shell is generated by increasing diagonal rods on the basis of Ribbed spherical reticulated shell. Its maximum displacement has decreased, but its maximum stress has increased. Under the same conditions, the maximum displacement and stress of Lamella spherical reticulated shell are smaller than Ribbed and Schwedler spherical reticulated shells.

(5) In the triangular pyramidal system, the grid division of Three-way grid, Kiewitt and Geodesic spherical reticulated shells is relatively uniform, and the mechanical behavior is better than the other three spherical reticulated shells

5. The shape optimization program design

The nodes distribution of partial double-layer spherical reticulated shells of pyramidal system has a regularity, which is determined by macroscopic surface shape and geometric parameters (*F*, *S*, *Kn*, *Nx*) of the structures. With regard to this kind of structures, cross-section optimization and shape optimization are carried out in order when conducting optimization design. Cross-section optimization adopts relative difference quotient algorithm (RDQA) based on discrete variables. Optimal cross-section size is sought by presetting macroscopic surface parameters. Then, on the basis of cross-section optimization, the optimal solution is got by changing macroscopic surface parameters with the goal of minimizing the total steel consumption, i.e., shape optimization.

5.1 Mathematical models of shape optimization

(1) Design variables

The cross-sectional area of the rod element A_i (i=1, 2, , m),

The volume of the node V_j (j=1, 2, , n).

(2) The objective function

The total weight of reticulated shells

$$\min W = \sum_{i=1}^{m} \rho_i l_i A_i + \sum_{j=1}^{n} \rho_j V_j \tag{3}$$

Where m is the number of rod elements; n is the number of nodes; A_i is cross-sectional area of the i-th rod element, (m^2); ρ_i, ρ_j are density of steel of rod elements and nodes respectively, (kg/m^3); l_i is geometry length of the i-th rod element, (m); V_j is volume of the j-th ball node, (m^3); The volume of hollow ball, $V_j=\pi d^2 t$, t is the wall thickness of welded hollow spherical joints, (mm).

(3) Constraint conditions

1) Deflection Constraints

$$\delta_{\max} \leq [\delta] \tag{4}$$

δ_{max} is the maximum calculated deflection, $[\delta]$ is the allowable deflection.
2) Strength constraints of the rods:
Pull rod

$$\sigma_i = \frac{N_i}{A_i} \leq [\sigma] \tag{5}$$

N_i is axial pull of the *i*-th pull rod, (*N*); $[\sigma]$ is the design strength.
Pressure rod

$$\sigma_i = \frac{N_i}{\varphi_i A_i} \leq [\sigma] \tag{6}$$

N_i is axial pressure of the *i*-th pressure rod, (*N*); φ_i is stability factor of the *i*-th pressure rod.
3) Slenderness ratio of the rods

$$\lambda_i = \frac{l_{0i}}{r_i} \leq [\lambda] \tag{7}$$

l_{0i} is geometry length of the *i*-th rod element, (m); r_i is cross-sectional radius of gyration of the *i*-th rod element, (m); λ_i is slenderness ratio of the *i*-th rod element, $[\lambda]$ is the allowable slenderness ratio.
4) Upper and lower constraints of cross-section of the rods

$$A_i \in \{A\} \tag{8}$$

$$V_j \in \{V\} \tag{9}$$

$$S_k \in \{S\} \tag{10}$$

$\{A\}$ is a variable discrete set of cross-sectional dimensions of the rods; $\{V\}$ is a variable discrete set of volume of the nodes; $\{S\}$ is a variable discrete set of structural geometry.
5) Constraints of the nodes:
Welded hollow spherical

$$D_{\min} \geq \frac{d_1 + d_2 + 2\alpha_n}{\theta} \tag{11}$$

d_1, d_2 is the outer diameter of two adjacent rods, (mm); θ is the angle between two adjacent rods, (rad); α_n is clear distance between adjacent rods in the spherical surface.

5.2 The two-stage optimization method

(1) The first-stage (cross-section) optimization:

The sequence two-stage optimization algorithm based on discrete variables is adopted. The first stage makes use of a one-dimensional search algorithm to process local constraints, such as stress constraints, stability constraints, slenderness ratio constraints, etc. The second stage takes advantage of relative difference quotient algorithm (RDQA) to handle whole constraints (Deng and Dong 1999).

Mathematical models (Lu *et al*. 2013, Sun *et al*. 2002) of cross-section optimization are as follows

$$\begin{aligned} &P_1 \quad \text{Seeking } A \\ &\min W = \sum_{i=1}^{m} \rho_i l_i(S) A_i + \sum_{j=1}^{n} \rho_j V_j \\ &s.t. \quad \sigma_{wi} \le [\sigma] \\ &\qquad \lambda_i \le [\lambda] \\ &\qquad x_i \in S_i \end{aligned} \tag{12}$$

(2) The second-stage (shape) optimization:

The aim is to seek optimal node locations along declining direction of the total weight, which can improve mechanical properties of the structures and provide an improved structural style for next round of cross-section optimization.

Mathematical models (Lu *et al*. 2013, Sun *et al*. 2002) of shape optimization are as follows

$$\begin{aligned} &P_2 \quad \text{Seeking } kn,\ nx \\ &\min W = \sum_{i=1}^{m} \rho_i l_i(kn,\ nx) A_i + \sum_{j=1}^{n} \rho_j V_j \\ &s.t. \quad \delta_{\max} \le [\delta] \end{aligned} \tag{13}$$

Given the range of *Kn* and *Nx*, optimal combination of *Kn* and *Nx* is searched with the goal of minimizing the total steel consumption of spherical reticulated shells

5.3 The design concept of shape optimization

As for partial double-layer spherical reticulated shells of pyramidal system, the number of rod elements and nodes are the main factors affecting the total weight of the structures. This study takes the total steel consumption of reticulated shells (including the weight of rods and nodes) as objective function. Meanwhile, *Kn* and *Nx* are taken as design variables (Lu *et al*. 2012). A shape optimization program is compiled in FORTRAN environment. The optimizer can use ANSYS to model, resolve and optimize in the background, so that the parameterization can be achieved. The specific process of shape optimization is as follows.

The optimum design program can be run after connecting with ANSYS. And the shape optimization is carried out by calling pre-processing and post-processing results of ANSYS directly. According to the optimized results, the real constants of rod elements in each group are modified, and they are read from lsjhao_result.txt. The new real constants are sent to the ANSYS for finite element analysis, then, the results are passed again to FORTRAN for optimization. The

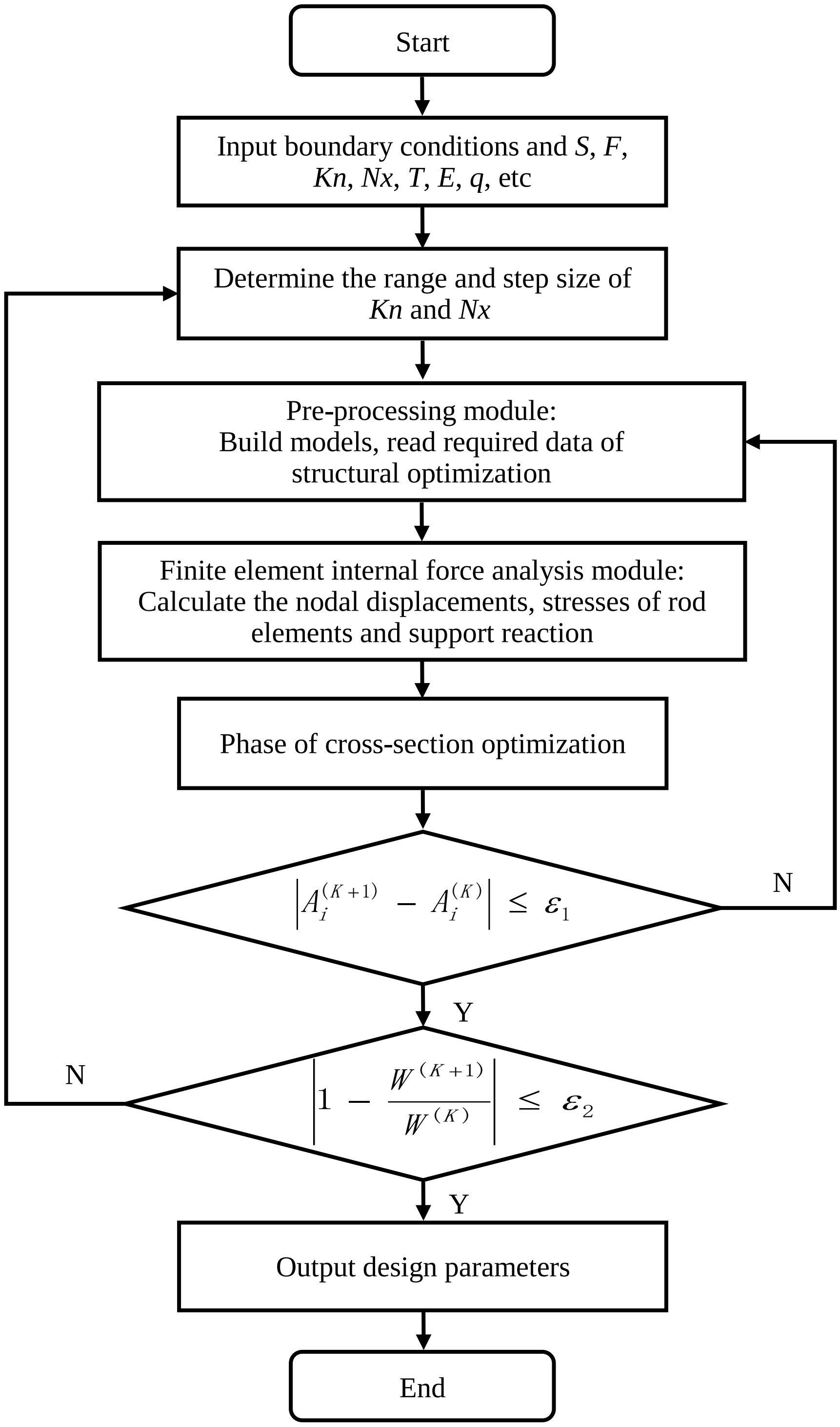

Fig. 17 Shape optimization flowchart of partial double-layer spherical reticulated shells of pyramidal system

cycle is kept going until it satisfies the constraints.

According to design concept of two-stage optimization (Sun *et al*. 2002, Chen 1989, Zhang and Hou 1998), the first-stage optimization, firstly the location and number of nodes are determined, meanwhile, the cross-sectional area of rods and the volume of nodes are used as design variables. Cross-section optimization is carried out by using one-dimensional search method and relative difference quotient method. The second-stage optimization, assumed the cross-sectional area of rods and the volume of nodes unchanged, taking *Kn* and *Nx* as design variables for shape optimization. Cross-section optimization and shape optimization are carried out simultaneously until the results converged. And optimal solution is obtained. Finally, the number of optimal grids is determined by optimal solution.

In order to present the process of shape optimization intuitively, Fig. 17 gives the flowchart of partial double-layer spherical reticulated shells of pyramidal system.

6. The results of shape optimization and discussion

The relevant parameters are unified, so that the optimized results are comparable (Lu *et al*. 2012). The rod elements of spherical reticulated shells adopt hot-rolling seamless pipe (calculated by YB 231-70). Constraints of spherical reticulated shells are simply supported. Uniform load q=2.35 KN/m^2, steel density ρ=7800 kg/m^3, elastic modulus E=2.06×10^5 Mpa, Poisson ratio ε=0.3, yield strength of steel [σ]=2.15×10^8 N/m^2. Optimal results of Ribbed, Schwedler and Lamella spherical reticulated shells with the span of 30 m~90 m are given in Tables 2-4. The optimized range of *Kn* is between 10 and 60, and the optimized range of *Nx* is between 6 and 20. Meanwhile, optimal results of Three-way grid, Kiewitt and Geodesic spherical reticulated shells with the span of 30 m~120 m are given in Tables 5-7. The optimized range of *Kn* is between 4 and 20, and the optimized range of *Nx* is between 6 and 20.

6.1 The results of shape optimization

The optimal results of six typical partial double-layer spherical reticulated shells of pyramidal system are shown in Tables 2-7.

Table 2 The optimal results of Ribbed partial double-layer spherical reticulated shells of quadrangular pyramid system

Type	Span (*m*)	The optimal steel consumption (*t*)	The optimal thickness (*m*)	The optimal rise to span ratio (*F/S*)	The number of optimal grids	
					Kn	*Nx*
Ribbed type	30	29.14	1.0	1/4	17	8
	40	48.98	1.0	1/4	26	8
	50	58.98	1.0	1/4	33	9
	60	69.38	1.0	1/4	37	12
	70	100.56	1.5	1/5	41	12
	80	127.55	1.5	1/5	49	15
	90	183.51	1.5	1/5	50	16

Table 3 The optimal results of Schwedler partial double-layer spherical reticulated shells of quadrangular pyramid system

Type	Span (m)	The optimal steel consumption (t)	The optimal thickness (m)	The optimal rise to span ratio (F/S)	The number of optimal grids	
					Kn	*Nx*
Schwedler type	30	33.39	1.0	1/5	16	10
	40	50.23	1.0	1/5	25	11
	50	65.35	1.0	1/5	31	12
	60	79.12	1.0	1/5	37	13
	70	98.56	1.5	1/5	42	14
	80	128.52	1.5	1/5	48	15
	90	185.24	1.5	1/5	52	16

Table 4 The optimal results of Lamella partial double-layer spherical reticulated shells of quadrangular pyramid system

Type	Span (m)	The optimal steel consumption (t)	The optimal thickness (m)	The optimal rise to span ratio (F/S)	The number of optimal grids	
					Kn	*Nx*
Lamella type	30	40.57	1.0	1/4	16	7
	40	59.24	1.0	1/4	25	8
	50	75.24	1.0	1/4	32	9
	60	95.84	1.0	1/4	37	12
	70	110.58	1.5	1/5	42	12
	80	145.88	1.5	1/5	48	14
	90	209.48	1.5	1/5	50	15

Table 5 The optimal results of Three-way grid partial double-layer spherical reticulated shells of triangular pyramid system

Type	Span (m)	The optimal steel consumption (t)	The optimal thickness (m)	The optimal rise to span ratio (F/S)	The number of optimal grids	
					Kn	*Nx*
Three-way grid type	30	38.47	1.0	1/4	6	10
	40	54.19	1.0	1/4	6	10
	50	75.42	1.0	1/4	6	11
	60	87.86	1.0	1/4	6	12
	70	97.50	1.0	1/5	6	13
	80	120.55	1.0	1/5	6	13
	90	157.14	1.5	1/5	6	15
	100	161.77	1.5	1/6	6	15
	110	201.61	1.5	1/6	6	16
	120	230.91	1.5	1/6	6	17

The following conclusions are reached from Tables 2-7:

(1) The optimal steel consumption of six typical partial double-layer spherical reticulated shells of pyramidal system increase with the span. As for spherical reticulated shells of different span and

Table 6 The optimal results of Kiewitt partial double-layer spherical reticulated shells of triangular pyramid system

Type	Span (*m*)	The optimal steel consumption (*t*)	The optimal thickness (*m*)	The optimal rise to span ratio (*F/S*)	The number of optimal grids	
					Kn	*Nx*
Kiewitt type	30	35.87	1.0	1/4	6	8
	40	51.76	1.0	1/4	6	8
	50	69.07	1.0	1/4	8	10
	60	85.42	1.0	1/4	6	11
	70	90.56	1.0	1/5	8	12
	80	112.56	1.0	1/5	8	14
	90	150.47	1.0	1/5	8	15
	100	150.94	1.5	1/6	8	16
	110	190.75	1.5	1/6	6	18
	120	218.78	1.5	1/6	8	18

Table 7 The optimal results of Geodesic partial double-layer spherical reticulated shells of triangular pyramid system

Type	S (*m*)	The optimal steel consumption (*t*)	The optimal thickness (*m*)	The optimal rise to span ratio (*F/S*)	The number of optimal grids	
					Kn	*Nx*
Geodesic type	30	34.42	1.0	1/4	5	9
	40	50.58	1.0	1/4	5	10
	50	67.99	1.0	1/4	5	10
	60	82.13	1.0	1/4	5	10
	70	87.11	1.0	1/5	5	12
	80	103.76	1.0	1/5	5	14
	90	138.45	1.0	1/5	5	15
	100	136.58	1.0	1/6	5	16
	110	185.42	1.5	1/6	5	17
	120	213.58	1.5	1/6	5	17

rise to span ratio, the number of optimal grids is existed after optimization, and at this moment, the total steel consumption is the least.

(2) The density of grid division has obvious implications for structural total steel consumption. The total steel consumption will increase rapidly whether the density is too dense or too sparse. *Nx* will increase as the span increases for the same type of spherical reticulated shell.

(3)When the span is between 30 m to 60 m, the optimal thickness is 1 m. Then, the optimal thickness will increase as the span increases.

(4) Schwedler spherical reticulated shell keeps its optimal rise to span ratio unchanged at 1/5. For other spherical reticulated shells, the optimal rise to span ratio will decrease as the span increases.

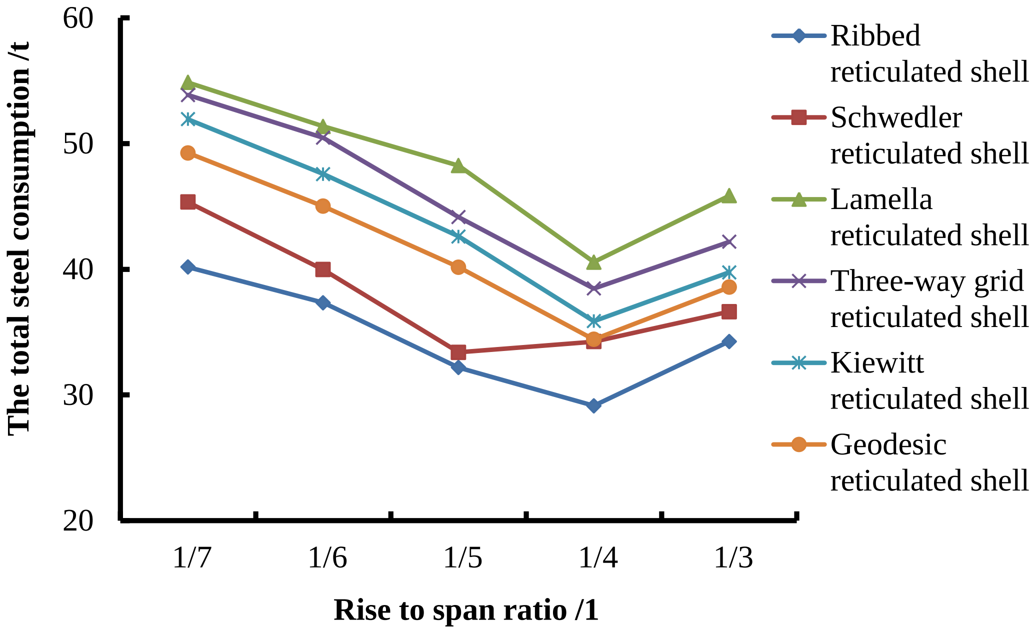

Fig. 18 The total steel consumption of six typical spherical reticulated shells when span is 30 m

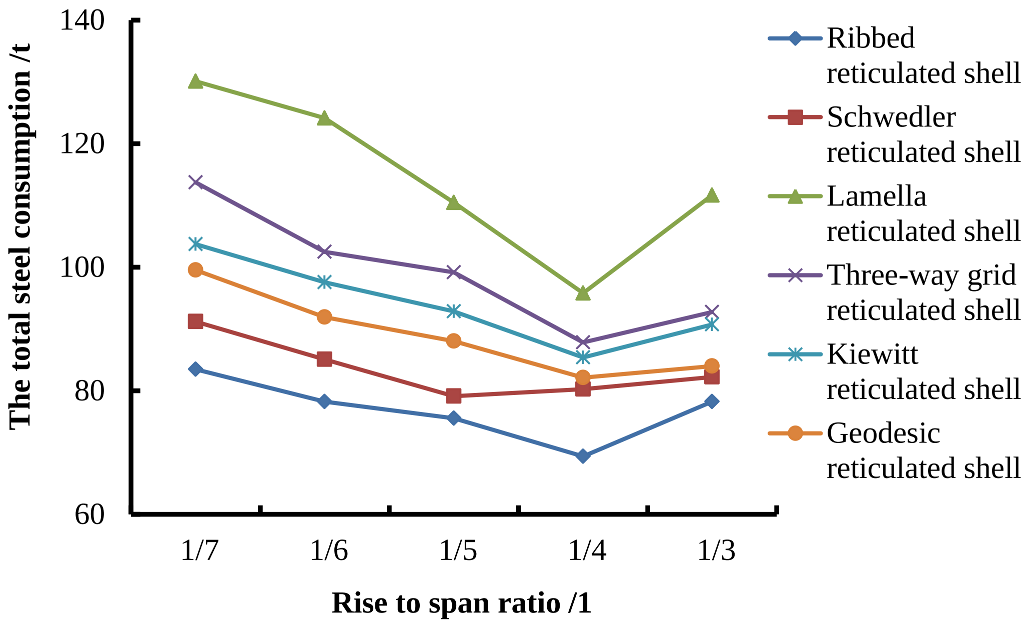

Fig. 19 The total steel consumption of six typical spherical reticulated shells when span is 60 m

6.2 Discussion

In order to compare change rule of total steel consumption for six typical partial double-layer spherical reticulated shells of pyramidal system after shape optimization, the total steel consumption with the span of 30 m, 60 m, 70 m, 90 m, 100 m and 120 m are shown by using curves.

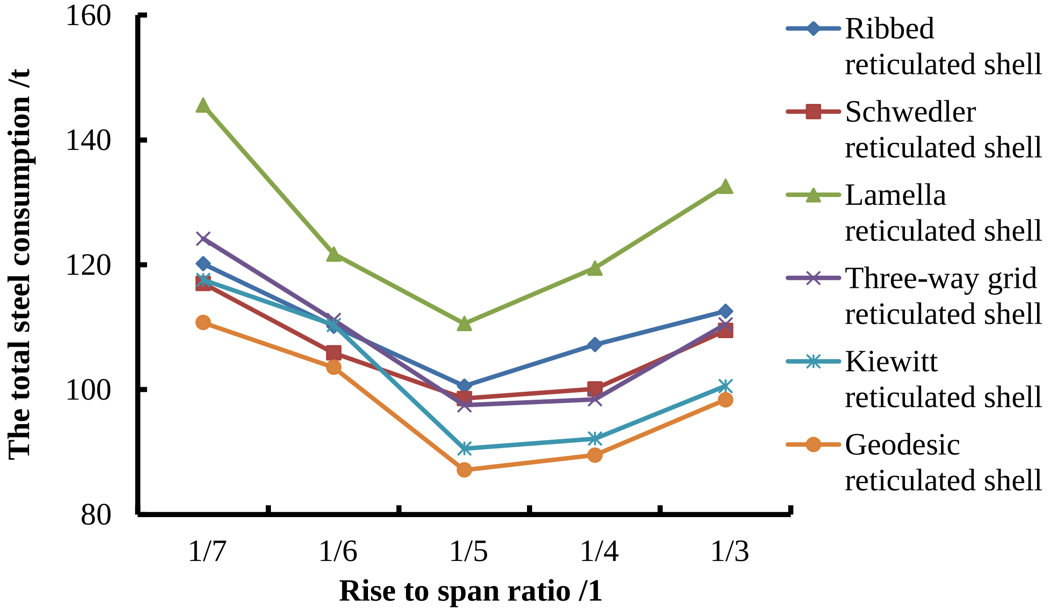

Fig. 20 The total steel consumption of six typical spherical reticulated shells when span is 70 m

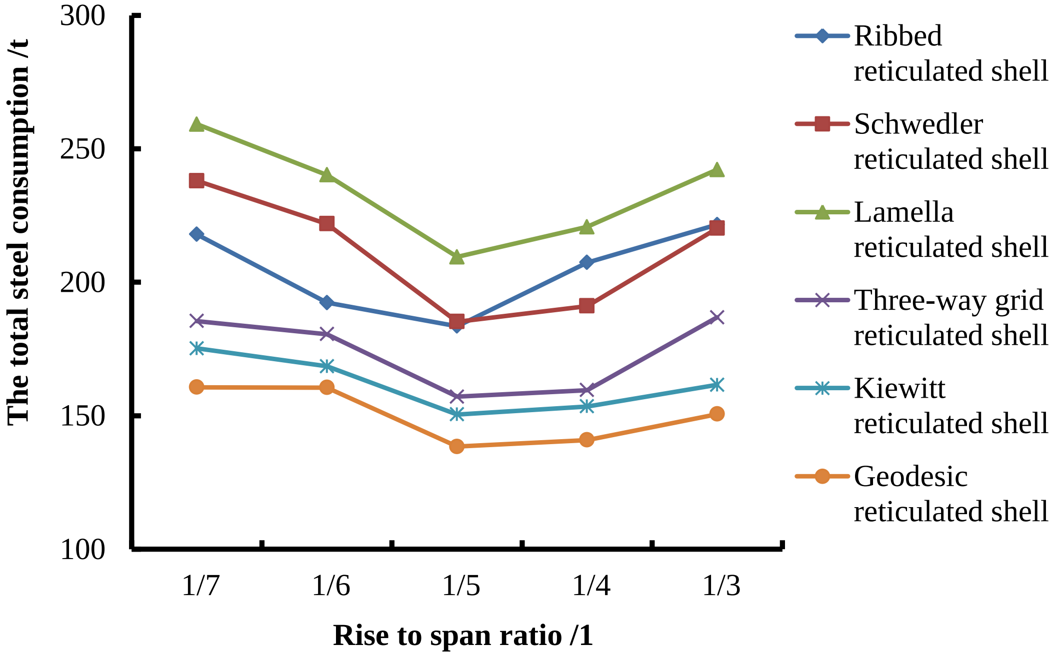

Fig. 21 The total steel consumption of six typical spherical reticulated shells when span is 90m

Under the same span and different rise to span ratio, the total steel consumption of six typical spherical reticulated shells after optimization are shown in Figs. 18-23.

The following conclusions are reached from Figs. 18-23:

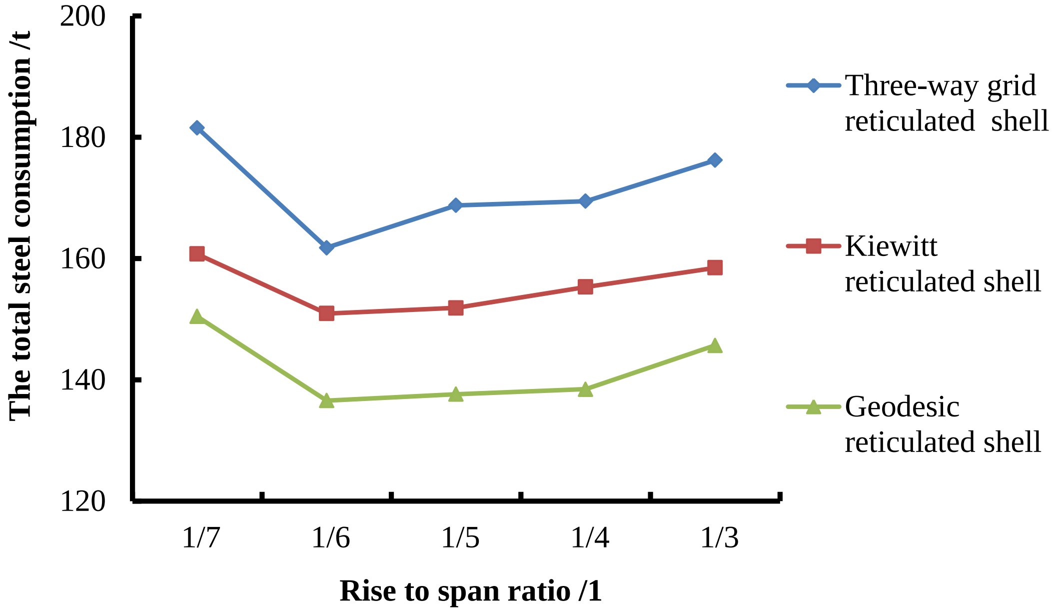

Fig. 22 The total steel consumption of six typical spherical reticulated shells when span is 100 m

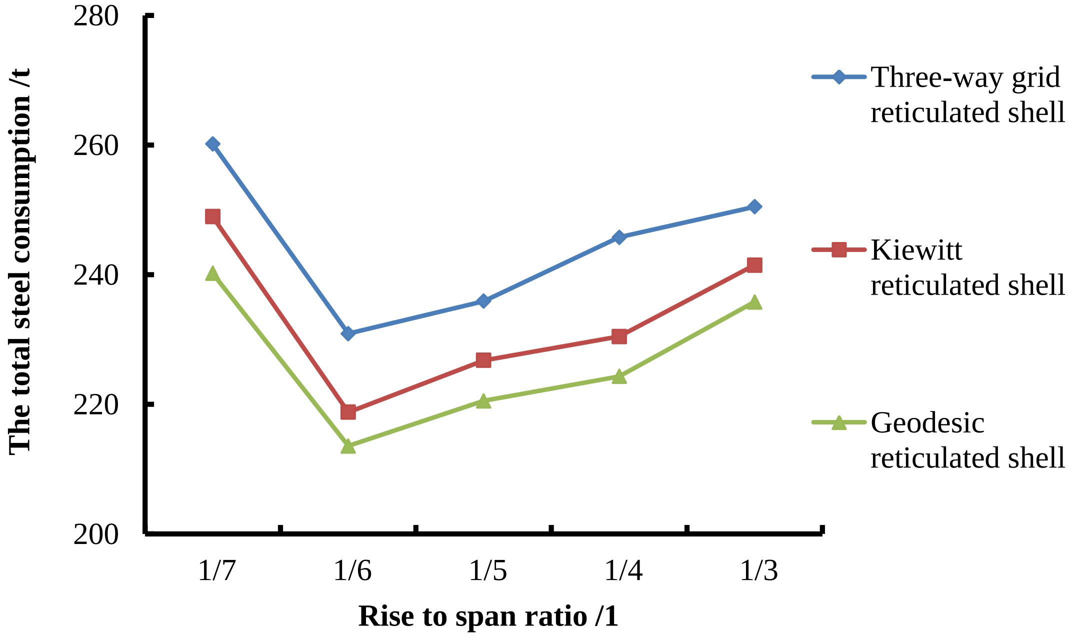

Fig. 23 The total steel consumption of six typical spherical reticulated shells when span is 120 m

(1) When the span is 30 m, it can be clearly seen from Fig. 18: With the increase of rise-span ratio, the total steel consumption of six typical partial double-layer spherical reticulated shells of pyramidal system decreases firstly, and then increases. The optimal rise to span ratio of Schwedler is 1/5, the other five spherical reticulated shells is 1/4. It is also concluded that the total steel consumption of Ribbed spherical reticulated shell is the least, followed by Schwedler spherical reticulated shell, and Lamella spherical reticulated shell is the largest.

(2) In the same way, when the span is 60 m (Fig. 19), the results are basically consistent with the analysis of Fig. 20. At this point, the total steel consumption of Lamella spherical reticulated shell is much larger than Ribbed spherical reticulated shell.

(3) When the span is between 70 m to 90 m, it can be clearly seen from Figs. 20-21: With the increase of rise-span ratio, the total steel consumption of six typical spherical reticulated shells decreases firstly, and then increases. When the rise to span ratio is 1/5, the total steel consumption is minimal. It also shows, the total steel consumption of Geodesic spherical reticulated shell is the least, followed by Kiewitt spherical reticulated shell, and Lamella spherical reticulated shell is also the largest.

(4) When the span is more than 90 m, the total steel consumption of Ribbed, Schwedler and Lamella spherical reticulated shells is much larger than the other three spherical reticulated shells. Therefore, the total steel consumption of the last three spherical reticulated shells is listed only. It can be seen from Figs. 22-23: With the increase of rise-span ratio, the total steel consumption of last three spherical reticulated shells decreases firstly, and then increases. When the rise to span ratio is 1/6, the total steel consumption is minimal. It is also concluded that the total steel consumption of Geodesic spherical reticulated shell is the least, followed by Kiewitt spherical reticulated shell, and Three-way grid is the largest.

(5) Overall, when the span is less than 60m, the difference of the total steel consumption of six typical spherical reticulated shells is small. Otherwise, the total steel consumption increases rapidly. When the span is 30 m, the difference of the total steel consumption between the maximum and minimum is 11 *t*. When the span is 60 m, the difference of the total steel consumption between the maximum and minimum is 27 *t*. The maximum difference has increased by nearly two times. And as the span increases, the difference gets bigger and bigger.

(6) Under the same span and rise to span ratio, after shape optimization, the most rapid increase in the total steel consumption is Lamella spherical reticulated shell increases. It shows that the mechanical behavior of the pyramidal system been set on the radical rods is better than the pyramidal system been set on latitudinal rods of Lamella type. So the mechanical property of Lamella spherical reticulated shell is inferior to the other five spherical reticulated shells.

(7) Under the certain span, the total steel consumption of six typical spherical reticulated shells changes with the changes of rise to span ratio. When the rise to span ratio is between 1/6 and 1/4, the figure is the lightest.

(8) In a word, when the span is not more than 60 m, the total steel consumption of Ribbed spherical reticulated shell is the minimum after shape optimization, followed by Schwedler spherical reticulated shell, and the difference of the total steel consumption between those two types is small. When the span is greater than 60 m, the total steel consumption of Geodesic spherical reticulated shell is the minimum after shape optimization, followed by Kiewitt spherical reticulated shell, and the difference of the total steel consumption between those two types is also small. Thus, from the viewpoint of economic aspect, Ribbed and Schwedler spherical reticulated shells can be used for small-span structures. Geodesic and Kiewitt spherical reticulated shells can be used for large, medium-span structures.

7. Conclusions

In the present study, as for six typical partial double-layer spherical reticulated shells of pyramidal system, an efficient parametric modeling method and a shape optimization method are proposed and compiled in APDL and FORTRAN language. The maximum stress and displacement of six typical spherical reticulated shells are analyzed. Shape optimization is carried out based on the objective function of the minimum total steel consumption and the restriction condition of strength, stiffness, slenderness ratio, stability. The variations of total steel consumption along with the span and span ratio are discussed with contrast to the results of shape optimization. The results show that:

• When the span is more than 60 m, from the viewpoint of internal force analysis and shape optimization, Kiewitt partial double-layer spherical reticulated shells of triangular pyramidal system is preferable. Thus, it can be widely used in large and medium-span structures.

• Similarly, as for Geodesic partial double-layer spherical reticulated shells of triangular pyramidal system, its mechanical behavior is second only to Kiewitt type, but its optimized results is better than Kiewitt type. Therefore, it can also be widely used in large and medium-span structures.

• For Ribbed partial double-layer spherical reticulated shells of quadrangular pyramidal system, its displacement is the largest after internal force analysis, but its mechanical properties can meet requirement. And when the span is not more than 60 m, the total steel consumption after shape optimization is the least. Thus, it can be widely used in small-span structures.

• For Schwedler partial double-layer spherical reticulated shells of quadrangular pyramidal system, its stress is the largest after internal force analysis, but its mechanical properties can meet requirement. And when the span is not more than 60 m, the total steel consumption after shape optimization is smaller. Thus, it can be widely used in small-span structures.

• As for Lamella partial double-layer spherical reticulated shells of quadrangular pyramidal system, it should not be generally adopted in actual projects because of its larger stress, displacement and total steel consumption.

• As for Three-way grid partial double-layer spherical reticulated shells of triangular pyramidal system, its mechanical behavior and optimized results are in the medium level, which can be used in medium-span structures.

Acknowledgements

We would like to acknowledge the financial support from the National Basic Research Program of China (973 Program, No.: 2013CB036000), the National Natural Science Foundation of China (Grant No.: 51479106, 41302225), the promotive research fund for excellent young and middle-aged scientists of Shandong Province (Grant No.: 2014GN028) and the China Postdoctoral Science Foundation (Grant No.: 2014M551908).

References

Chen, L.Z. (1989), *The Optimal Method of Discrete Variable-Principle and Application*, China Machine Press, Beijing, China.

Chen, Z.H. and Liu, H.B. (2009), *APDL Parametric Calculation and Analysis*, China Water Power Press, Beijing, China.

Deng, H. and Dong, S.L. (1999), "Shape optimization of spatial reticulated shell structures", *J. Zhejiang Univ. (Eng. Sci.)*, **33**(4), 371-375.

Dong, S.L. and Yao, J. (2003), "Future and prospects of reticulated shells", *Spatial Struct.*, **9**(1), 31-34.

Durgun, İ. and Yildiz, A.R. (2012), "Structural design optimization of vehicle components using cuckoo search algorithm", *Mater. Test.*, **54**(3), 185-188.

Emmanuel Nicholas, P., Padmanaban, K.P. and Vasudevan, D. (2014), "Buckling optimization of laminated composite plate with elliptical cutout using ANN and GA", *Struct. Eng. Mech.*, **52**(4), 815-827.

Gong, S.G. and Xie, G.L. (2010), *ANSYS Parametric Programming and Command Manual*, China Machine Press, Beijing, China.

He, Y.J., Qi, D.L. and Dong, S.L. (2001), "Application of chaos optimization algorithm in the optimization of double-layer cylindrical latticed shell", *J. China Coal Soc.*, **26**(6), 663-666.

He, Y.J., Qi, D.L. and Dong, S.L. (2002), "Application of genetic algorithm in the optimization of double-layer cylindrical latticed shell", *J. China Coal Soc.*, **26**(6), 663-666.

Jenkins, W.M. (1991), "Towards structural optimization via the genetic algorithm", *Comput. Struct.*, **40**(5), 1321-1327.

Jenkins, W.M. (1991), "Structural optimization with the genetic algorithm", *Struct. Eng.*, **69**(24), 418-422.

Jenkins, W.M. (1997), "On the application of natural algorithms to structural design optimization", *Eng. Struct.*, **19**(4), 302-308.

JGJ7 (2010), *Technology Procedures of Space Grid Structures*, China Building Industry Press, Beijing, China.

Kaveh, A. and Ahmadi, B. (2014), "Sizing, geometry and topology optimization of trusses using force method and supervised charged system search", *Struct. Eng. Mech.*, **50**(3), 365-382.

Kaveh, A. and Zolghadr, A. (2014), "A new PSRO algorithm for frequency constraint truss shape and size optimization", *Struct. Eng. Mech.*, **52**(3), 445-468.

Levy, R., Hanaor, A. and Rizzuto, N. (1994), "Experimental investigation of prestressing in double-layer grids", *Int. J. Space Struct.*, **9**(1), 21-26.

Lu, X.Y., Zhao, X.W. and Chen, S.Y. (2013), *The Optimization of Reticulated Shell Structures Based On Discrete Variables*, Building Industry Press, Beijing, China.

Lu, X.Y., Zhao, X.W. and Huang, L.L. (2012), "Shape optimizing design of kiewiti spherical reticulated shell", *Adv. Mater. Res.*, **424**, 324-329.

Luo, Z., Zhang, N., Gao, W. and Ma, H. (2012), "Structural shape and topology optimization using a meshless Galerkin level set method", *Int. J. Numer. Meth. Eng.*, **90**(3), 369-389.

Rajan, S.D. (1995), "Sizing, shape, and topology design optimization of trusses using genetic algorithm", *J. Struct. Eng.*, **121**(10), 1480-1487.

Rahami, H., Kaveh, A. and Gholipour, Y. (2008), "Sizing, geometry and topology optimization of trusses via force method and genetic algorithm", *Eng. Struct.*, **30**(9), 2360-2369.

Saka, M.P. (1991), "Optimum design of steel frames with stability constraints", *Comput. Struct.*, **41**(6), 1365-1377.

Saka, M.P. and Kameshki, E.S. (1998), "Optimum design of nonlinear elastic framed domes", *Adv. Eng. Softw.*, **29**(7), 519-528.

Salajegheh, E. and Vanderplaats, G.N. (1993), "Optimum design of trusses with discrete sizing and shape variables", *Struct. Optim.*, **6**(2), 79-85.

Shang, X.J. and Qiu, F. (2005), *ANSYS Structural Finite Element Senior Analysis Method and Sample Applications*, China Water Power Press, Beijing, China.

Shen, Z.Y. and Chen, Y.J. (1996), *Grid and Lattice Shell*, Tongji University Press, Shanghai, China.

Sun, H.C., Chai, S. and Wang, Y.F. (2002), *Structural Optimization with Discrete Variables*, Dalian University of Technology Press, Dalian, China.

Svanberg, K. (1987), "The method of moving asymptotes-a new method for structural optimization", *Int. J. Numer. Meth. Eng.*, **24**(2), 359-373.

Thrall, A.P., Zhu, M., Guest, J.K., Paya-Zaforteza, I. and Adriaenssens, S. (2014), "Structural optimization of deploying structures composed of linkages", *J. Comput. Civil Eng.*, **28**(3), 04014010.
Vyzantiadou, M.A., Avdelas, A.V. and Zafiropoulos, S. (2007), "The application of fractal geometry to the design of grid or reticulated shell structures", *Comput. Aid. Des.*, **39**(1), 51-59.
Wang, C.W. and Tang, G. (2006), "Sectional optimum design of single-layer lattice shells considering structural stability", *Spatial Struct.*, **12**(3), 31-34.
Wu, W., Petrini, L., Gastaldi, D., Villa, T., Vedani, M., Lesma, E. and Migliavacca, F. (2010), "Finite element shape optimization for biodegradable magnesium alloy stents", *Ann. Biomed. Eng.*, **38**(9), 2829-2840.
Xu, J., Yang, S.S. and Diao, Y.S. (2006), "Optimized design of single-layer reticulated shell", *Spatial Struct.*, **12**(3), 35-37.
Yas, M.H., Shakeri, M. and Ghasemi-Gol, M. (2007), "Two-objective stacking sequence optimization of a cylindrical shell using genetic algorithm", *Scientia Iranica*, **14**(5), 499-506.
Yildiz, A.R. (2013), "Comparison of evolutionary-based optimization algorithms for structural design optimization", *Eng. Appl. Artif. Intell.*, **26**(1), 327-333.
Zhang, B.H. and Hou, C. (1998), *Optimization Design of Civil Structures*, Tongji University Press, Shanghai, China.
Zhang, D.L., Lu, X.Y., Chen, S.Y. and Ge, Z.L. (2013), "Parametric design and stress characteristic of K6-type triangular pyramid system domes", *J. Shandong Jianzhu Univ.*, **28**(5), 425-431.
Zhang, D.L. (2014), "Partial double reticulated shell shape optimization and stability analysis of pyramidal system", M.S. Dissertation, Shandong Jianzhu University, Ji'nan.
Zhang, N.W. and Dong, S.L. (2003), "Optimum design of single-layer lattice shells considering the effect of geometrical nonlinearity", *Spatial Struct.*, **9**(1), 31-34.

CC